

Wilfried Wunderlich*, Lothar Machon** and Gerhard Sauthoff

(Max-Planck-Institut für Eisenforschung GmbH, Max-Planck-Str. 1, D-4000 Düsseldorf 1)

Dislocation Analysis at Crack Tips at Phase Boundaries in an Intermetallic NiAl – NbNiAl Alloy

Dedicated to Professor Dr. rer. nat. Wolfgang Pitsch on the occasion of his 65th birthday

A quasibinary eutectic alloy which consists of the intermetallic phases NiAl with B2 structure and NbNiAl – a Laves phase with C14 structure – shows improved strength at temperatures up to 1200 °C compared to pure NiAl. The brittleness of the NbNiAl phase, however, causes microcracking during deformation at room temperature and at elevated temperatures. With TEM observations the interaction of cracks with the phase boundary NiAl/NbNiAl was studied in detail. In some cases the crack energy was absorbed in NiAl by the formation of a plastic zone. The detailed dislocation analysis showed that seven slip systems were activated in total in NiAl including the <100>{310} system. The results are discussed in the light of other crack tip studies and are compared to macroscopic deformation experiments in NiAl.

Versetzungsanalyse an Rißspitzen an Phasengrenzen in einer intermetallischen NiAl–NbNiAl-Legierung

Eine quasibinäre eutektische Legierung, die aus den beiden intermetallischen Phasen NiAl mit B2-Struktur und NbNiAl – eine Laves-Phase mit C14-Struktur – besteht, zeigt im Vergleich zu einphasigem NiAl eine verbesserte Festigkeit bis zu Temperaturen von 1200 °C. Die Sprödigkeit der NbNiAl-Phase verursacht jedoch Mikrorißbildung bei Verformung bei Raumtemperatur und erhöhten Temperaturen. Mit TEM-Untersuchungen wurde die Wechselwirkung von Mikrorissen mit den Phasengrenzen im Detail untersucht. In einigen Fällen wurde die Energie des Risses in NiAl absorbiert, indem eine plastische Zone gebildet wurde. Die detaillierte Versetzungsanalyse zeigt, daß insgesamt sieben Gleitsysteme aktiviert worden sind, unter anderem auch das <100>{310}-System. Die Ergebnisse werden mit anderen Rißspitzenuntersuchungen und makroskopischen Verformungsexperimenten verglichen.

1 Introduction

Among other intermetallic compounds the NiAl phase has a perspective for applications as high-strength material [1 to 4] because of the high melting point, the good oxidation resistance and the relatively low density. It is well established that single crystals of NiAl show a high anisotropy. The non-<100> oriented crystals (soft orientation) are much more ductile than the <100> oriented crystals (hard orientation) [5 to 9]. The low tensile ductility of polycrystalline NiAl at room temperature has been attributed to the insufficient number of activated slip systems – <001>{110}, <001>{100} – to satisfy the von Mises criterion [7, 9, 10] although several authors found evidence for activation of other slip systems, e.g. <100>{210} [6, 13]. Even the pencil glide mechanism has been proposed [7, 9], i.e. the slip plane becomes ill-defined and slip takes place on any plane with the slip direction <001> as zone axis [14]. At high temperatures or high deformation rates other slip systems (<111>{123}, <111>{112}, <111>{110} [6, 15 to 17] and <110>{110} [8, 9, 18]) have been found. In compression tests ductility is observed, but in tension brittle fracture mostly occurs. The interaction of slip and fracture is not quite well understood.

Additions of Nb to NiAl are expected to increase the strength and in particular the creep resistance [3]. With more than 1 at.% Nb the NbNiAl phase with the hexagonal C14 structure ($MgZn_2$-type Laves phase) is formed [17, 19] leading to a quasibinary eutectic system NiAl-NbNiAl. Two-phase alloys containing NiAl and NbNiAl are supposed to show an improved creep resistance because NbNiAl has a high strength at temperatures up to 1400 °C [2, 3, 20, 21]. A problem, however, is the brittleness of this phase.

The mechanical behaviour of NiAl-NbNiAl alloys has been reported preliminarily [2, 3] and is described separately [20, 21]. The properties of the alloy of this study are summarized briefly in Table 1. The compressive yield strength (0.2 % proof stress at deformation rate $\dot{\varepsilon} = 10^{-4}$ 1/s) of the Ni40Al39Nb21 alloy was found as 357 MPa at 1100 °C. This strength is much higher than that of pure stoichiometric NiAl with 30 MPa. NiAl containing 0.6 at.% Nb in solution has a compressive yield strength of 68 MPa. The NbNiAl phase exhibits a compressive yield strength of 592 MPa. At room temperature the alloy fractured in a brittle manner with a strength of more than 1500 MPa. The ultimate compressive stress was 1407 MPa at 800 °C (1 % strain), 1075 MPa at 900 °C (> 12 % strain),

* now with Max-Planck-Institut für Mikrostrukturphysik, Weinberg 2, D-O-4050 Halle

** now with Kontinentale Tiefbohrung, D-8486 Windischeschenbach

Table 1. Chemical composition and properties of the studied NbNiAl-NiAl alloy with 28 vol.% NiAl and 72 vol.% NbNiAl (after [20 to 22]).

material	NiAl ("ductile")	NiAl with 1 at.% Nb	NbNiAl ("brittle")	NbNiAl-NiAl
crystal structure	B2	B2	C14	B2 + C14
Ni content [at.%]	50	50	33	40
Al content [at.%]	50	49.4	33	39
Nb content [at.%]		0.6	33	21
compressive 0.2 % proof stress [MPa] at 1100 °C [20, 21]	30	68	592	357
K_{IC} [MPam$^{1/2}$] (RT) [22]	4		2	4
Thermal expansion coefficient				
– parallel to c-axis	$1.5 \cdot 10^{-5}$ K^{-1}		$1.10 \cdot 10^{-5}$ K^{-1}	
– perpendicular to c-axis	$1.5 \cdot 10^{-5}$ K^{-1}		$0.99 \cdot 10^{-5}$ K^{-1}	
– polycrystalline specimen	$1.5 \cdot 10^{-5}$ K^{-1}		$1.05 \cdot 10^{-5}$ K^{-1}	

642 MPa at 1000 °C (> 12 % strain) and 200 MPa at 1200 °C (> 15 % strain). Detailed creep experiments reveal a similar brittle-to-ductile transition. K_{IC} measurements (Table 1) which are described elsewhere [22] showed values of about 4 MPa$\sqrt{m}$ at room temperature for both the pure NiAl and the Ni40Al39Nb21 alloy. NbNiAl is rather brittle with a K_{IC} value of about 2 MPa$\sqrt{m}$.

The aim of the present work is to study the microstructure and especially the dislocation configuration in the NiAl phase in front of microcracks at the phase boundaries between NiAl and NbNiAl. The results are compared to other studies of dislocations at crack tips.

2 Experimental Details

A NiAl-NbNiAl alloy with the composition Ni-39 at.% Al-21 at.% Nb was produced by electron-beam melting. A eutectic microstructure with spheroidal NiAl grains surrounded by the NbNiAl phase was obtained with an average grain size of 500 µm. By chemical analysis the impurity content was found to be extremely low with < 50 ppm O_2, < 30 ppm N_2, < 10 ppm S. EDX-SEM measurements showed that the NiAl phase contains at least 0.6 at.% Nb in solid solution (Tab. 1). The measured Ni and Al contents correspond to the equilibrium contents of the two phases. From the ingots specimens with dimensions $6 \times 6 \times 10$ mm^3 were cut by spark erosion for creep tests.

After the creep experiments the specimens were studied by light microscopy. With a special etchant (16 vol.% HNO_3, 16 vol.% (40 HF), 68 vol.% glycerin) the two phases could be distinguished clearly. The preparation for TEM was difficult since the NbNiAl phase is rather brittle and grinding had to be done carefully. The specimens were thinned by conventional twin jet polishing with a HNO_3 – methanol (1:3) solution with 30 V at – 25 °C. Dimple grinding before polishing improved the size of the thin areas. The Philips EM420 electron microscope was equipped with a ± 60°/30° double tilt specimen holder for easy dislocation analysis.

The thermal expansion coefficient was measured for NiAl as well as for NbNiAl. NiAl single crystals were available which showed isotropic thermal expansion values (Table 1). The pure NbNiAl phase was solidified directionally with the c- axis parallel to the growth direction. The thermal expansion coefficient parallel and perpendicular to the c-axis is significantly different (Table 1). Measurements with randomly oriented polycrystals yielded mean values.

3 Results

The Ni40Al39Nb21 alloy contained about 72 vol.% NbNiAl phase (bright phase in Fig. 1) and about 28 vol.% NiAl phase. Figure 1a shows the microstructure after deformation at 400 °C. The NbNiAl phase contains many cracks which continue in the NiAl phase. At 800 °C (Fig. 1b) the cracks which have

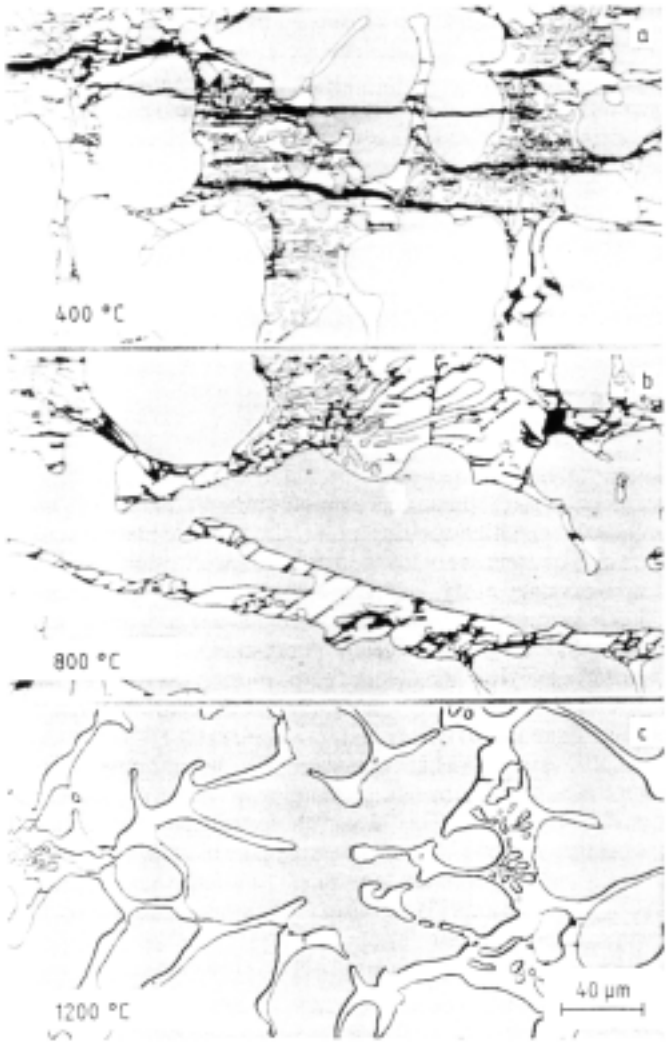

Fig. 1a to c. Light micrograph of the Ni40Al39Nb21 alloy after creep deformation at various temperatures: (a) 400 °C, (b) 800 °C, (c) 1200 °C [20, 21].

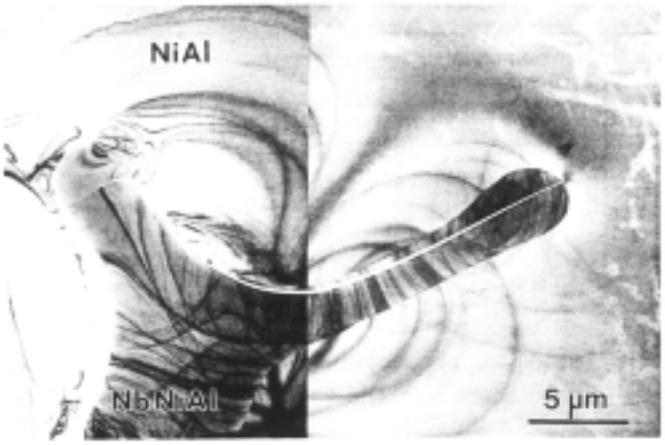

Fig. 2. Intragranular crack in NbNiAl phase along the phase boundary of NiAl.

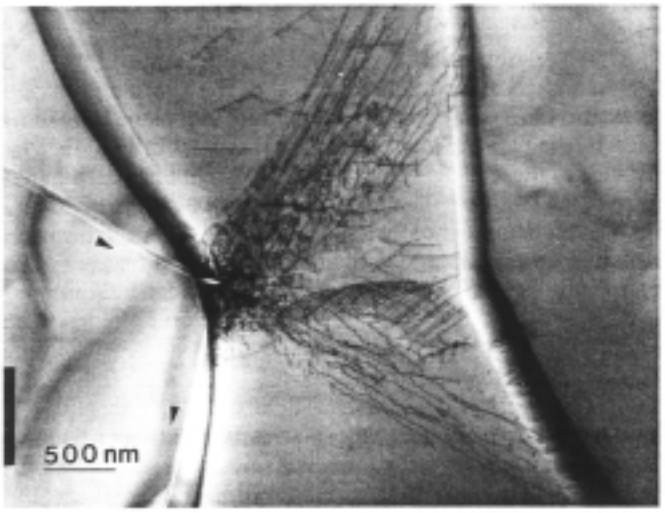

Fig. 3. Reflected crack at the NiAl phase boundary with angle of incidence below 55° and plastic zone in the NiAl phase.

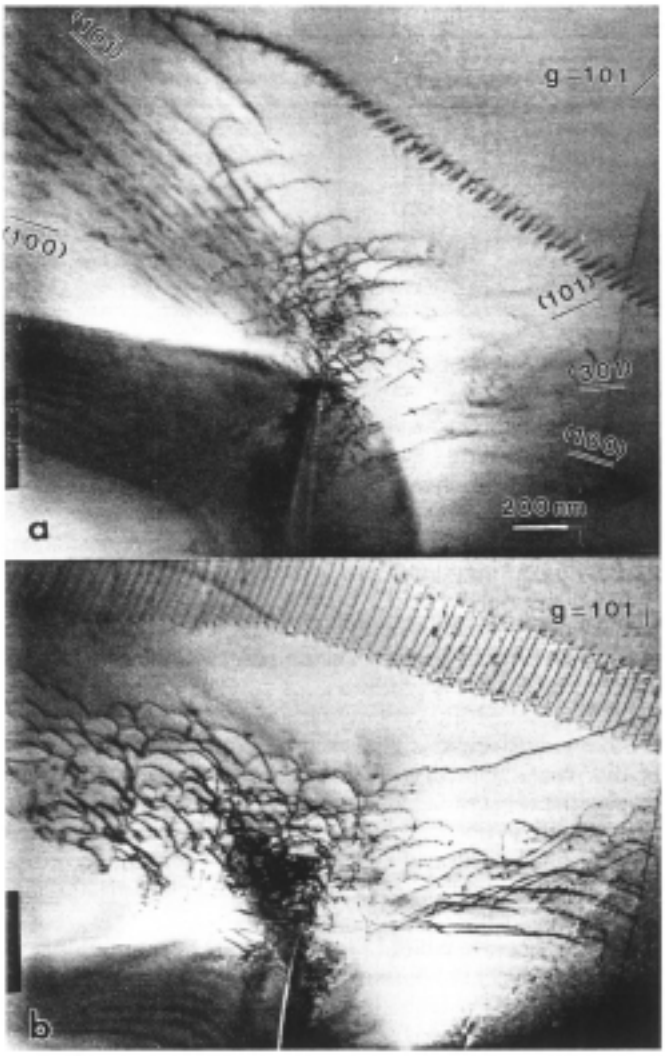

Fig. 4a to b. Plastic zone in NiAl under different imageing conditions: (a) $\vec{g} = [10\bar{1}]$, (b) $\vec{g} = [101]$.

been formed in the NbNiAl phase have been stopped at the phase boundary of NiAl. At 1200 °C (Fig. 1c) the deformation was purely plastic and no cracks were observed.

TEM investigations were performed after deformation at 1000 °C and 1200 °C. Altough in the optical microscope microcracks were not visible, i.e. they were absent or smaller than the resolution, the TEM foils contained intergranular cracks in the NbNiAl phase (Fig. 2). The cracks did not follow any crystallographic plane in the NbNiAl phase, but were curved without any preferred orientation. In the case of Fig. 2 the crack was deflected near the phase boundary. The crack seems to follow the phase boundary at a distance of about 500 nm. This leads to the conclusion that the phase boundary possesses a higher fracture strength than the NbNiAl phase.

About twenty cracks were studied in detail. If the angle between the crack plane and the phase boundary exhibits a sharp angle between 10° and about 55° the crack is "reflected" at the phase boundary. Figure 3 shows that in these cases the angle of incidence is nearly equal to the angle of reflection. The crack propagation direction is marked by arrows. In most cases dislocations are formed in the NiAl phase starting from the intersection of the crack with the phase boundary.

Small particles of the metastable Nb_2NiAl phase with $L2_1$ structure (Heusler type) have been formed within the NiAl during cooling after creep at 1000 °C for more than 20 h. The reason for this is the decreasing solubility of Nb in NiAl with decreasing temperature. Nucleation occurs preferentially on previous dislocations. The plastic zone at crack tips, however, does not contain such particles. Therefore, the observed dislocations at crack tips must have been formed after the creep experiment. By careful comparison of light micrographs and TEM micrographs of selected specimen regions it was found that most cracks were formed during deformation and cooling and not during TEM-specimen preparation. New cracks caused by preparation were running between the two phases whereas the original ones had a direction perpendicular to the phase boundaries.

If the angle of incidence at the phase boundaries exceeds a critical value of about 55°, the crack stops at the phase boundary. The energy is absorbed in the plastic zone which is formed in the NiAl phase. Figure 4 shows an example with a crack incidence angle of about 90° and a plastic zone of about 8 µm size. A detailed dislocation analysis was performed in this case by tilting with at least six different image vectors $\vec{g}$. Two examples are shown in Fig. 4 with $\vec{g} = [10\bar{1}]$(a) and $\vec{g} = [101]$(b). Two types of dislocations were created, i.e. most dislocations had a Burgers vector $\vec{b} = [010]$ and a few had $\vec{b} = [001]$. In Fig. 4a the specimen was tilted in such way that the normal direction of the image plane (zone axis) is nearly perpendicular to the slip plane of the $\vec{b} = [010]$ dislocations. In

Table 2. Activated slip systems at the crack tip in NiAl.

Burgers vector	slip plane	line vector	curvature	number of dislocations N	density ρ	Schmid factor
[010]	(100)	10°-screw	middle	3	middle	0.17
[010]	(10$\bar{1}$)	10°-screw	very strong	12	very high	0.45
[010]	(101)	10°-screw	weak	9	high	0.26
[010]	(301)	mixed	weak	8	middle	0.06
[010]	(100)	10°-edge	weak	ca. 5	middle	0.17
[001]	($\bar{1}$10)	mixed	strong	ca. 5	low	0.22
[001]	($\bar{3}$10)	mixed	weak	ca. 20	high	0.33

Fig. 4b the specimen was tilted to have a zone axis near [010]. This means that the $\vec{b} = [010]$ dislocations are imaged with their residual contrast as is indicated by the weak double line contrast which fulfils the condition $\vec{g} \cdot \vec{b} = 0$. Only the few $\vec{b} = [001]$ dislocations appear with full contrast since for them $\vec{g} \cdot \vec{b} \neq 0$. Often (cf. upper part of Fig. 4) small-angle grain boundaries were observed which were formed during creep deformation at high temperatures without relation to cracks.

The line vectors of the dislocations were estimated by using the trace method [23] in stereographic projections for different zone axes. From the line vectors the slip planes can be obtained by the cross product $\vec{l} \times \vec{b}$. The analysis showed that in total seven slip systems were activated, as summarized in Table 2. Dislocations with near edge character were found on slip planes with steep angles to the crack plane, whereas those with near screw character lie on planes with sharp angle. The dislocation lines were curved, but no evidence was found for cross slip or dislocation reactions. Most [010] dislocations lie on the [10$\bar{1}$] slip plane, but also other slip planes ({100} and {310}) were found.

The schematic sketch in Fig. 5 illustrates the three-dimensional arrangement of the slip planes in the NiAl phase in front of the crack tip. The crack plane is indicated with the notation of the NiAl phase. For a better understanding the slip planes of the dislocations with the two types of Burgers vectors are drawn separately although they penetrate each other in three dimensions. Since the {310} slip planes seem to be rather unusual they were checked in a different way. As mentioned above, the micrograph of Fig. 4b was obtained with a zone axis near $\vec{b} = [010]$. With this imaging condition the slip planes of the $\vec{b} = [010]$ dislocations appear as planar traces since they contain the zone axis. The angle of 18° between the trace of the (301) plane and the trace of the (100) plane corresponds to the correct value. Therefore, it can be stated that {310} slip planes are activated.

The dislocations in the left part of Fig. 4a show a rather small radius of curvature. The zone axis in this image is nearly perpendicular to the (10$\bar{1}$) plane which was found as slip plane for these dislocations. The strong curvature with a radius R of at least 30 nm indicates a rather high internal stress with strong dislocation pinning. With $\tau \approx 0.5b \cdot G/R$ (with $G = 63$ GPa [20]) a stress of about 300 MPa can be estimated. This slip system also had the largest density of dislocations ρ (see Table 2) which was estimated by counting the dislocations on that slip system and considering the distance of the slip planes. Each dislocation lies on a separate but parallel slip plane as is indicated by the parallel lines of residual contrast in Fig. 4b. The distance of these planes increases slightly with increasing distance of the crack tip. The lowest distance was measured as 50 nm. The high number of dislocations in this slip system can be explained by estimating the Schmid factor. As a first approximation, the stress field in front of the crack tip can be supposed to be a tensile stress perpendicular to the crack plane. The Schmid factor can be calculated by $S = \tau/\sigma = \cos\Theta \cos\lambda$ with the assumption that the stress acts along [1$\bar{3}$3] direction which is the normal of the crack plane. The results for each slip system are shown in Table 2. Slip systems with a higher Schmid factor exhibit higher dislocation densities, and also the dislocation curvatures are stronger in these slip systems. Hence, the results are selfconsistent. In pure single crystals of NiAl [24] some preparation cracks also showed a (0$\bar{3}$1) slip plane of emitted dislocations.

4 Discussion

Two-phase alloys containing the NiAl phase and the NbNiAl phase showed improved mechanical properties compared to pure NiAl. Obviously, the high volume fraction of NbNiAl strengthens the alloy. The improvement in the K_{IC} values is probably due to crack deflection.

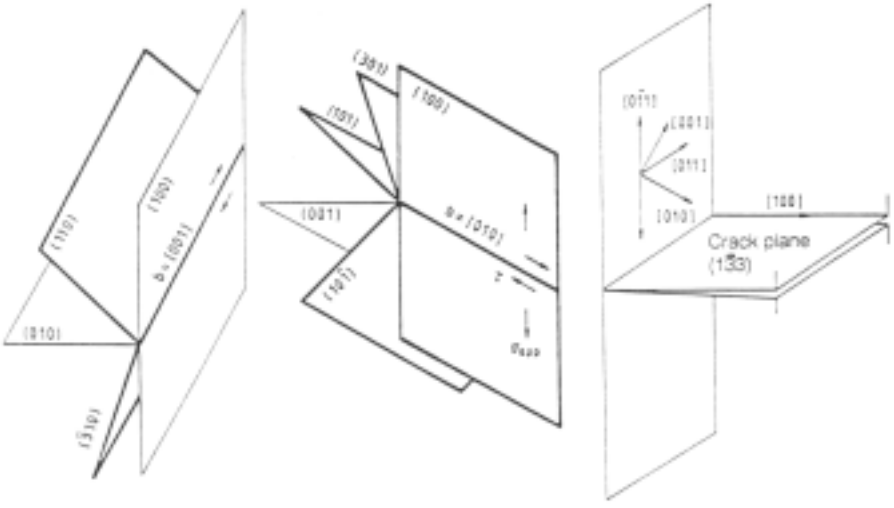

Fig. 5. Slip planes and Burgers vectors in the plastic zone in NiAl of Fig. 4 as well as crack plane in NbNiAl (schematically, the notation refers to the NiAl lattice).

The NiAl phase possesses a slightly higher strength (Table 1) if about 1 at.% Nb is dissolved. In this case the dislocations are strongly bent with a high curvature. Obviously, clusters of Nb atoms act as obstacles for dislocations since precipitated particles could not be detected. Pinning by forest dislocations can be excluded because with various imageing conditions only dislocations were found which had been emitted from the crack tip. Hence, the solid solution hardening contribution by the Nb atoms is rather large. In specimens with supersaturated NiAl formation of metastable $L2_1$ Ni_2NbAl particles was observed in NiAl (for details see [20, 21]).

The NbNiAl containing alloy has been used to study the plastic zone at crack tips in NiAl. Microcracks observed by light microscopy are formed within the NbNiAl phase after deformation during the subsequent cooling from the high temperature. The microcrack density observed by light microscopy was found to increase with decreasing deformation temperature. Hence, it can be concluded that internal stresses cause the microcracking which results from the large difference of the thermal expansion coefficients of NbNiAl and NiAl (Table 1) and from the thermal gradients [20, 21]. The microcrack formation is supposed to occur at temperatures far below the testing temperature (1000 °C) since otherwise the forces due to differences in thermal contraction would not be large enough to exceed the cleavage strength of NbNiAl. The brittle-to-ductile transition temperature of NbNiAl was found to be around 1000 °C. Above this temperature internal stresses in NbNiAl can be relaxed by dislocation movements. Therefore, microcracking is assumed to take place much below 1000 °C. A lower limit presumably is the temperature of about 400 °C because specimens deformed at that temperature showed brittle cracks even in the NiAl phase. Single phase NiAl is known to be brittle at low temperatures, but experiments in NiAl single crystals showed dislocation emission at crack tips in TEM specimens which were produced during the thinning process at room temperature [24]. Therefore, it cannot be excluded that the plastic zone in NiAl has formed at room temperature at least on a microscopic scale in the thin TEM foils. Additional microcracks in NbNiAl may be formed during TEM specimen preparation by relaxation of internal stresses since the neighbouring grains are removed. Due to the difference in thermal expansion coefficients (Table 1) the NbNiAl phase is under compression at room temperature.

The curvature of the cracks shows that the NbNiAl phase has no preferred cleavage plane. The phase boundary between the NbNiAl and NiAl phase was found to be stronger than the brittle NbNiAl phase. Obviously, the neighborhood of NiAl results in long-range image forces. Effects of the chemical composition can be excluded since EDX line scans across the phase boundary in the TEM showed a sudden change in the Nb, Ni and Al concentration to the bulk values. The angle of incidence plays an important role for the crack propagation at the phase boundary. Below a limit of 55° cracks are reflected with an angle equal to the angle of incidence. The formation of a plastic zone in NiAl means that a part of the kinetic energy is dissipated even if a propagating crack is reflected at the phase boundary.

Plastic zones at crack tips are formed in NiAl if the angle between crack plane and phase boundary is above 55°. The dislocation density decreases with increasing distance from the crack tip as found by Appel et al. at crack tips in MgO [25]. Compared to metals the behaviour of dislocations at the crack tip in NiAl is between that of fcc and bcc alloys. By in-situ straining experiments in the TEM Ohr [26] found emission of screw dislocations on planes coplanar to the plane of the mode III crack in fcc metals (Cu, Ni, steel, Al). Although the cracks at the phase boundaries NiAl/NbNiAl are predominatly mode I cracks, screw dislocations were observed on slip planes with sharp angles (near coplanar) to the crack plane (Table 2, Fig. 5). Most of the slip planes, however, had a steep angle to the crack plane containing dislocations with edge character.

Dislocations theories of fracture [26 to 29] intend to describe and understand the brittle-to-ductile transition of materials. The macroscopic fracture behaviour is described with K_{app}, the stress intensity factor from the applied stress, and is explained by microscopic deformation mechanisms with k_{tip}, the local stress intensity factor at the crack tip. In the present work the plastic zone in NiAl contained more than 62 dislocations with seven slip systems. The position and distance of them to the crack tip can be estimated. However, the three-dimensional dislocation configuration leads to complicated interactions of stress fields which makes an analysis difficult.

Slip systems in NiAl in front of a crack tip have not yet been investigated before in detail. With single crystals mainly compression tests were performed [5, 7, 15, 16] where activation of $<100>\{110\}$ and $<100>\{100\}$ slip systems and also $<100>\{210\}$ [6, 13] was found. Baker et al. [12] predicted the occurrence of additional slip systems with $<100>\{hk0\}$. Results of the present work clearly show that $<100>$ dislocations are activated on $\{100\}$ and $\{110\}$ as well as on $\{310\}$ slip planes. The latter plane is observed here for the first time. The results clearly show that dislocations on $\{310\}$ planes cannot be described by slip steps on different $\{110\}$ planes as suggested by Ball and Smallman [10]. They are presumably activated only under special loading conditions as in the stress field at crack tips. The occurrence of the $<001>\{310\}$ slip system means that its activation energy is of the order of that of the $<100>\{100\}$ and $<100>\{110\}$ slip systems, at least it is smaller than the energy for fracture. In the stereographic projection the $\{310\}$ planes are situated rather close to the previously published $\{210\}$ planes, i.e. they can easily be mixed up with each other. According to these results slip planes in NiAl seem to be not as well-defined as in other crystals. Hence, the consideration of pencil glide with its variety of slip planes seems to be reasonable. This is supported, too, by regarding the slip in $<111>$ direction. Such Burgers vectors were not found under the experimental conditions of the present work, since only at lower temperatures or high deformation rates the slip systems $<111>\{123\}$, $<111>\{112\}$, $<111>\{110\}$ were observed [16, 17]. In Cr-doped NiAl enhanced nucleation and motion of $<111>$ dislocations on $\{112\}$ planes has been found even at room temperature [30]. The variety of slip planes for both $<100>$ and $<111>$ Burgers vectors indicates the possibility of pencil glide for NiAl.

The findings of this work show the activation of seven different slip systems in NiAl with six of them being independent on a microscopic scale. This is more than sufficient to fulfill the von Mises criterion. Bulk specimens of NiAl are known to behave in a brittle manner in tensile tests, but recently Hahn et al. [31] found also room temperature ductility of NiAl even in polycrystalline material if the stoichiometric composition is exactly established. Obviously, the influence of the chemical composition is critical and further experiments with different alloy compositions are required for a detailed understanding.

5 Conclusions

In the two-phase alloy NiAl/NbNiAl cracks are formed in the brittle NbNiAl-phase during cooling from the test temperature (1000 °C) to room temperature.

If a crack propagating in the brittle phase NbNiAl meets the phase boundary of NiAl it is reflected if the angle of incidence is below 55° which indicates a higher strength of the phase boundary compared with the pure NbNiAl phase.

At angles of incidence above 55° the crack is stopped at the interface by producing a plastic zone in the NiAl phase which can be analysed by TEM. Two types of Burgers vectors were found, [010] and [100], operating on six independent slip systems which is more than enough to fulfill the von Mises criterion for general homogeneous deformation. The presence of the slip plane {310} is evidence for the occurrence of pencil glide in NiAl with 1 at.% Nb.

The work was supported financially by Bundesministerium für Forschung und Technologie (BMFT) which is gratefully acknowledged. The authors wish to thank Mrs. Erika Bartsch for her assistance and in particular for the difficult TEM specimen preparation.

Literature

1. *Sauthoff, G.:* Z. Metallkd. *77* (1986) 654–666.
2. *Sauthoff, G.:* Z. Metallkd. *80* (1989) 337–344.
3. *Sauthoff, G.:* Z. Metallkd. *81* (1990) 855–861.
4. *Darolia., R.:* J. Materials (1991) 44–49.
5. *Wasilewski, R. J.; Butler, S. R.; Hanlon, J. E.:* Trans. Met. Soc. AIME *239* (1966) 1357–1364.
6. *Pascoe, R. T.; Newey, C. W. A.:* phys. stat. sol. *29* (1966) 357–366.
7. *Ball, A.; Smallman, R. E.:* Acta Metall. *14* (1966) 1349–1355.
8. *Field, R. D.; Lahrman, D. F.; Darolia, R.:* Acta Metall. Mater. *39* (1991) 2961–2969.
9. *Field, R. D.; Lahrman, D. F.; Darolia, R.:* Acta Metall. Mater. *39* (1991) 2951–2959.
10. *Ball, A.; Smallman, R. E.:* Acta Metall. *14* (1966) 1517–1526.
11. *Yoo, M. H.; Takasugi, T.; Hanada, S.; Izumi, O.:* Mat. Trans. JIM *31* (1990) 435–442.
12. *Baker, I.; Schulson, E. M.:* Metall. Trans. A *15A* (1984) 1129–1136.
13. *Miracle, D. B.:* Acta Metall. Mater. *39* (1991) 1457–1468.
14. *Grooves, G. W.; Kelly, A.:* Philos. Mag. *8* (1963) 877–887.
15. *Lloyd, C. H.; Loretto, M. H.:* phys. stat. sol. *39* (1970) 163–170.
16. *Loretto, M. H.; Wasilewski, R. J.:* Philos. Mag. *23* (1971) 1311–1328.
17. *Munroe, P. R.; Baker, I.:* Scripta Metall. *23* (1989) 495–499.
18. *Dollar, M.; Dymek, S.; Hwang, S. J.; Nash, P.:* Scripta Metall. *26* (1992) 29–34.
19. *Kumar, K. S.:* Int. Mat. Rev. *35* (1990) 293–327.
20. *Machon, L.:* Dr. rer. nat. Thesis, RWTH Aachen (1992).
21. *Machon, L.; Sauthoff, G.:* to be published.
22. *Reuss, S.; Vehoff, H.:* Scripta Metall. Mater. *24* (1990) 1021–1026.
23. *Edington, J. W.:* Practical Electron Microscopy, Philips Technical Library (1975).
24. *Wunderlich, W.; Vehoff, H.:* to be published.
25. *Appel, F.; Messerschmidt, U.; Kuna, M.:* phys. stat. sol. (a) *55* (1979) 529–536.
26. *Ohr, S. M.:* Mat. Sci. Eng. *72* (1985) 1–35.
27. *Chiao, Y. H.; Clarke, D. R.:* Acta Metall. *37* (1989) 203–219.
28. *Brede, M.; Haasen, P.:* Acta Metall. *36* (1988) 2003–2018.
29. *Kohlhoff, S.; Gumbsch, P.; Fischmeister, H. F.:* Philos. Mag. A *64* (1991) 851–878.
30. *Miracle, D. B.; Russell, S.; Law, C. C.:* Mat. Res. Sym. Proc. *133* (1988) 225–230.
31. *Hahn, K. H.; Vedula, K.:* Scripta Metall. *23* (1989) 7–12.

(Received: January 16, 1992)